crystals

MDPI

Article

On the Behavior of Ferroelectric Liquid Droplets in the Vicinity of a Ferroelectric Solid

Raouf Barboza, Sameh Bahwi, Stefano Marni and Liana Lucchetti *

Dipartimento SIMAU, Università Politecnica delle Marche, Via Brecce Bianche, 60131 Ancona, Italy; r.barboza@univpm.it (R.B.); bahwi.sameh@gmail.com (S.B.); stefanomarni@gmail.com (S.M.)
* Correspondence: l.lucchetti@univpm.it

Abstract: We analyzed the behavior of sessile ferroelectric liquid droplets in the vicinity of a pyroelectrically charged ferroelectric crystal, an experimental configuration that allows testing the recently observed coupling between the polarizations of the fluid and solid materials, in conditions of no direct contact. Results demonstrate that polarizations' coupling also exists in this configuration and has two distinct effects. Specifically, it gives rise both to an electromechanical instability of the liquid droplets consisting in the sudden ejection of interfacial fluid jets, and to a slow droplet motion toward the ferroelectric solid driven by a dielectrophoretic force. The two effects can possibly be separated, depending on the droplet size.

Keywords: ferroelectric nematic liquid crystals; lithium niobate; pyroelectric effect

Citation: Barboza, R.; Bahwi, S.; Marni, S.; Lucchetti, L. On the Behavior of Ferroelectric Liquid Droplets in the Vicinity of a Ferroelectric Solid. *Crystals* **2023**, *13*, 750. https://doi.org/10.3390/cryst13050750

Academic Editors: Vladimir Chigrinov and Aleksey Kudreyko

Received: 7 April 2023
Revised: 27 April 2023
Accepted: 28 April 2023
Published: 30 April 2023

1. Introduction

The recent discovery of the ferroelectric nematic liquid crystal phase (N_F) marks a revolution in material science [1]. Indeed, more than 100 years after the Born prediction [2], the elusive polar nematic phase—the first ferroelectric fluid with a workable viscosity—has been found in two distinct compounds, the firsts of a whole class of novel liquid crystalline materials. This is an important discovery, because the combination of fluidity and polar coupling to electric fields is opening the gate to a whole new world of phenomena, which are rapidly becoming the focus of the liquid crystal and soft material scientific communities [3–15]. In this scenario, we recently performed experiments aimed at characterizing the behavior of sessile N_F droplets on ferroelectric solid substrates [16] and found that the combination of fluidity and polarity gives rise to an electromechanical instability induced by the coupling of the LC polarization with the polarization of the solid substrate. This latter can be induced either pyroelectrically by temperature variation [16] or photovoltaically through light irradiation [17,18]. The coupling between the polarization in the solid and fluid materials induces the accumulation of surface charges on the droplet–air interface, which can give rise to repulsive forces that become unsustainable by the surface tension. The resulting instability takes the form of an abrupt expulsion of polarized fluid jets, whose electrically charged tips are repelled by the droplet. The tips themselves are unstable and often bifurcate, leading to a cascade of branched dynamic fluid jets and eventually disrupting into new small droplets.

Such a polarization coupling is a new phenomenon, and is observable thanks to the peculiar fluid nature of the ferroelectric nematic phase. Being new, its characterization and understanding are desirable from both the point of view of the fundamental research and of the possible future applications. Indeed, this effect might pave the way to the realization of novel hybrid liquid/solid devices as, for example, ferroelectric memories, supercapacitors, micro and optofluidic platforms for the control of complex ferroelectric fluids, and electrically or optically controlled droplet dispensers. Moreover, it might provide the basis for electrohydromechanical applications, such as soft robotics.

With the aim of further analyzing this effect, here, we characterize the behavior of sessile ferroelectric liquid droplets deposited on glass substrates and placed in the vicinity of a pyroelectrically charged ferroelectric crystal. This experimental configuration allows for testing the coupling between the polarizations of the fluid and solid materials in conditions of no direct contact between the two, and thus is different from those of both ref. [16] and [17], where the droplets lay directly on a ferroelectric substrate. Results demonstrate that polarization coupling also exists in this configuration and has two distinct effects. Indeed, it is responsible for both the electromechanical instability leading to the sudden ejection of interfacial fluid jets, and a slow droplets' motion toward the ferroelectric solid driven by a dielectrophoretic force. According to [16], the interaction between the polarizations of the two ferroelectric materials is mediated by the fringing field E_f generated by the pyroelectric effect in the vicinity of the ferroelectric crystal surface; our measurements thus set a value for the range of action of E_f in the used experimental conditions.

Worthy of note, the behavior of liquid crystalline materials in combination with ferroelectric substrates has also been studied in the case of the conventional nematic phase in several different configurations [19–22]. The ability of substrate charging to affect the LC average molecular orientation has been demonstrated; however, no effect comparable to that observed with ferroelectric nematic LCs was reported.

2. Materials and Methods

The ferroelectric liquid crystal used in this work is 4-[(4-nitrophenoxy)carbonyl]phenyl-l2,4-dimethoxybenzoate (RM734). It was synthesized as described in [1], and its structure and phase diagram have already been reported [1,6,16]. In this compound, the ferroelectric nematic (N_F) phase appears through a second order phase transition upon cooling from the conventional higher temperature nematic (N) phase and exists in the range of 133 °C > T > 80 °C [6,16]. The spontaneous polarization **P** of RM734 is either parallel or antiparallel to the molecular director **n**, defining the average orientation of the molecular axis, and exceeds 6 $\mu C/cm^2$ at the lowest temperature in the N_F phase [1].

The RM734 droplets were obtained following two steps. First, a small amount of RM734 powder is deposited at room temperature on a clean glass slide and heated to 150 °C to create a melt. To create the initial droplets, a cold stainless needle is dipped into the melt and retracted, so that the droplet on its tip solidifies at contact with the surrounding air. To increase the size of the RM734 "pearl", rapid (to avoid re-melting) successive dipping is performed. Then, the pearl is remolten into a droplet on the glass substrate. The glass slide is then cooled down to room temperature so that solidified droplets can be peeled off and reused on the proper substrate. The size of the droplets is controllable (size before peeling vs. size of the remolten droplet) and is measured by means of a calibration slide. The average diameter ranges from 400 to 200 µm. For the experiments described here, the obtained droplets were deposited on unrubbed glass substrates. Bare glass and fluorolink-coated glass substrates were used. Fluorolink was selected, as it features extremely low surface coupling of RM734 molecules [6], thus providing a good comparison with the behavior of RM734 droplets on bare glass. Fluorolink coating was obtained as described in [6]. Before droplet deposition, glass substrates were slowly heated up to T = 200 °C, corresponding to the RM734 isotropic phase, and a rectangular ferroelectric crystal with a size of 10 mm × 5 mm was placed on top of it, as sketched in Figure 1. Successively, T was decreased down to 80 °C with a cooling rate of (0.30 ± 0.05) °C/s.

As ferroelectric crystals, we used 900 µm thick z-cut lithium niobate (LN) slabs. Experiments were performed on iron-doped substrates containing 0.1% mol. of iron with a reduction factor R, defined as the ratio $Fe^{2+}/Fe^{3+,}$ of 0.02. The bulk spontaneous polarization P_{LN} of LN crystals along the [0001] z-axis is of the order of 70 $\mu C/cm^2$ and does not depend significantly on T in the explored range, since its Curie temperature is much higher (≈1140 °C). The huge bulk polarization of LN does not, however, translate to a huge surface charge density because of very efficient compensation mechanisms at the z-cut surfaces, lowering the equilibrium surface charge to only about 10^{-2} $\mu C/cm^2$ [23]. When

temperature variations are induced, the surface charge of LN can significantly increase because of the pyroelectric effect [24], a transient phenomenon observable during and shortly after the variation and due to the slow free charge relaxation in LN. The pyroelectric coefficient of undoped LN is of the order of 10^{-4} C/m^{2}K at room temperature [25,26], and increases by one order of magnitude around 100 °C for both undoped and iron-doped crystals [27]. Given the temperature used in our experiments, and dictated by the RM734 phase diagram, we can thus expect an induced surface charge density of the order of 1 μC/cm^2, for T variations of a few degrees ramped in a short time compared to the LN charge relaxation. LN crystals were placed on top of the heated glass substrates, and RM734 droplets were positioned directly on the glass at a controlled distance from the LN slab (Figure 1). The distance between the droplet edge and the edge of the LN crystal was measured by a calibration slide with an experimental error of ±5 μm. The distance was adjusted by sliding the crystal away from/towards the droplet. Polarized optical microscope (POM) observations during the cooling were carried out, and videos of the droplet's behavior were recorded with a rate of 25 frames per second. Note that both the glass substrates and the z-cut LN crystals appear to be dark under crossed polarizers. For this reason, a full wave plate was added to the microscope to increase the contrast of the images.

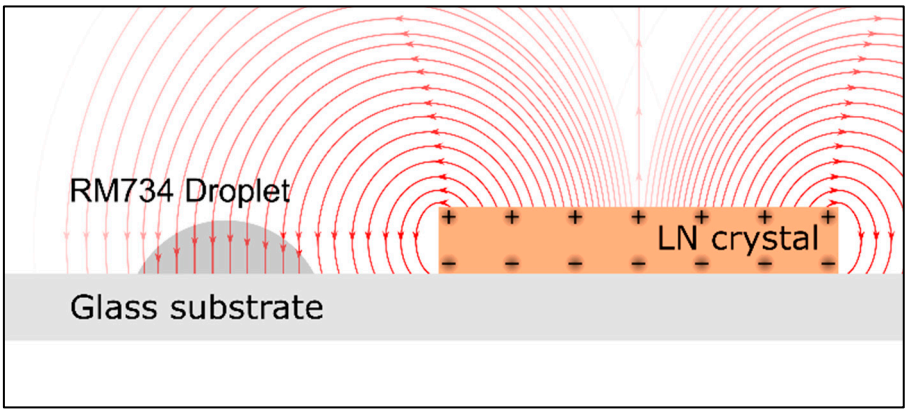

Figure 1. Sketch of the experimental arrangement. The orange full lines indicate the fringing field E_f generated by pyroelectric charging of the LN crystal. Lighter colors refer to weaker field.

3. Results

The electromechanical instability of RM734 ferroelectric droplets deposited on ferroelectric substrates [16] has been interpreted as being due to the coupling between the polarization of the ferroelectric fluid and the polarization of the ferroelectric solid substrate. This coupling is mediated by the fringing field generated by the pyroelectric charging of LN [16], which exists outside the crystal with a certain extension, as sketched in Figure 1. Therefore, it can be expected that RM734 droplets are affected by the LN polarization even in conditions of no direct contact between the two materials. This has been indeed observed and is reported in Figure 2, where several frames extracted by Video S1, available in the S.I., demonstrate the behavior of a RM734 ferroelectric droplet on a bare glass substrate, upon cooling down to 80 °C. A 400 μm droplet is positioned so that its edge is at a distance d_E = 150 μm from the border of the LN crystal, as measured as detailed in the previous section (Figure 2a). About 4.4 s after the transition to the N_F phase, the droplet undergoes a deformation toward the LN slab (Figure 2b), followed by several other transient deformations and by the ejection of very small fluid jets that are almost immediately retracted (Figure 2c,d). The deformations become bigger and affect a larger part of the droplet as the temperature decreases (Figure 2e) and eventually result in the electromechanical instability described in [16], consisting of the emission of fluid jets that run over the substrate and branch with several levels of ramifications (Figure 2f–h). Jets are initially ejected mainly from regions closer to the LN crystal, in the direction of the LN itself (Figure 2f) and later

extend to the whole droplet rim (Figure 2g). Interestingly, additional fluid jets come from the liquid crystalline material that enters the region between the LN and glass, forming a thin LC layer (Figure 2g,h). We interpret these jets in analogy to those produced by the electromechanical instability of ferroelectric RM734 droplets that is due to the imbalance between the surface tension and the electrostatic energy accumulated by the ferroelectric fluid in contact with the charged ferroelectric solid [16]. The changes in color of the LN crystal close to the border indicate a non-uniform variation of the birefringence that we understand as being due to a nonuniform pyroelectric charging. This might be due to a not optimal isolation of the temperature controller (hot-stage) or to a piezoelectric deformation of the crystal.

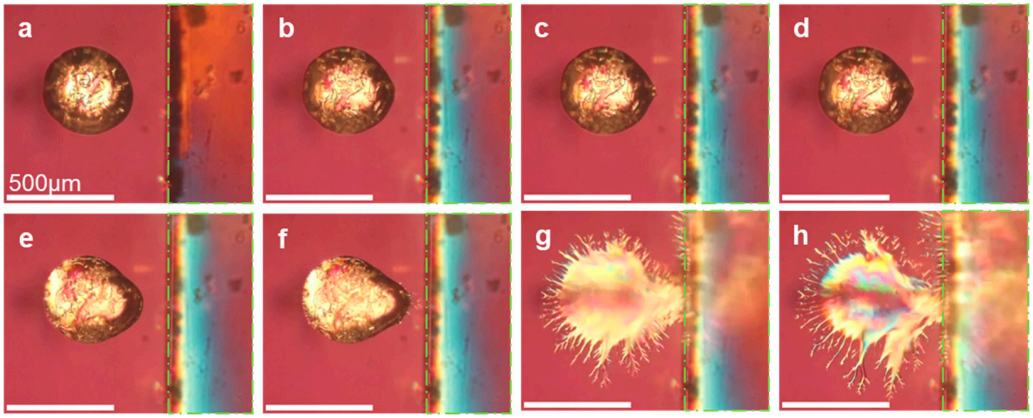

Figure 2. RM734 ferroelectric droplet on a bare glass substrate upon cooling from 130 to 80 °C. The green dashed line marks the edge of a LN crystal positioned on the right-hand side of the droplet, at 150 µm from the droplet rim (**a**). Upon lowering the temperature, the droplet undergoes a deformation toward the LN slab (**b**). This is followed by several other transient deformations that in some cases are accompanied by the ejection of very short fluid jets (**c**) that are almost immediately retracted (**d**). Continuing to cool, the deformations become bigger (**e**) and eventually lead to the droplet's electromechanical instability (**f**,**g**). (**h**) Initial droplet diameter D = 400 µm.

Varying the initial distance d_E between the droplet edge and LN border has two effects. On the one hand, it results in a change of the temperature at which the first deformation is observed, which decrease as d_E increases. On the other hand, it affects the electromechanical instability, which also occurs at a lower temperature and is generally less violent upon increasing d_E.

Interestingly, jets' ejection does not always occur in the direction of the LN slab. Figure 3 shows an example of fluid jets emitted from the droplet side opposite to the LN crystal, in the case of a fluorolink-coated glass substrate. Noteworthy, while droplet deformation toward the LN crystal is not necessarily associated with jet ejection, the latter is, on the contrary, always connected to a deformation of the droplet rim. This suggests that the observed deformation might be the result of two different effects: the electromechanical instability induced by the rearrangement of the droplet polarization and the droplet attraction toward the LN crystal.

To test this hypothesis, we measured the possible motion of the droplets in the direction of the LN crystal by tracking the position of a specific point identified as the droplet center. The results are reported in Figure 4a, where the distance d between the center of a RM734 ferroelectric droplet and the LN edge is plotted as a function of time. The initial instant t = 0 has been chosen a few frames before the beginning of motion, which starts at T = 105 °C, which is well inside the N_F phase. The shape of the curve suggests the presence of both a pinning force that acts as a static friction and of a friction of dynamic nature dependent on the droplet velocity, which leads to a uniform motion with constant velocity for a certain interval before the droplet stops. Such a dynamic friction is most probably a viscous

force due to the internal fluid motion, in analogy to that observed in the case of smaller RM734 ferroelectric droplets moving on LN substrates due to localized photovoltaic LN charging [17]. Noteworthy, the motion ends before the droplet reaches the border of the LN crystal, as it is also visible in the three images on the right-hand side of the graph.

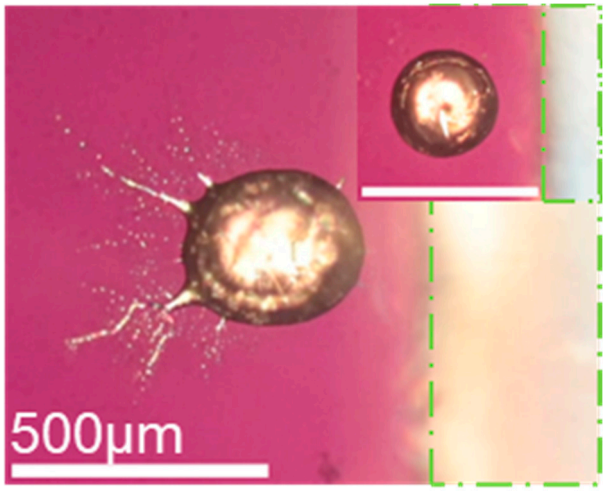

Figure 3. RM734 ferroelectric droplet on a fluorolink-coated glass substrate during an instability event (T = 100 °C). The green dashed line marks the edge of a LN crystal positioned on the right-hand side of the droplet, at 140 μm from the droplet rim. The fluid jets are mainly ejected in the direction opposite to the LN slab and are emitted from the droplet's left side. The inset shows the same droplet right after the N/N_F transition. Initial droplet diameter D = 280 μm.

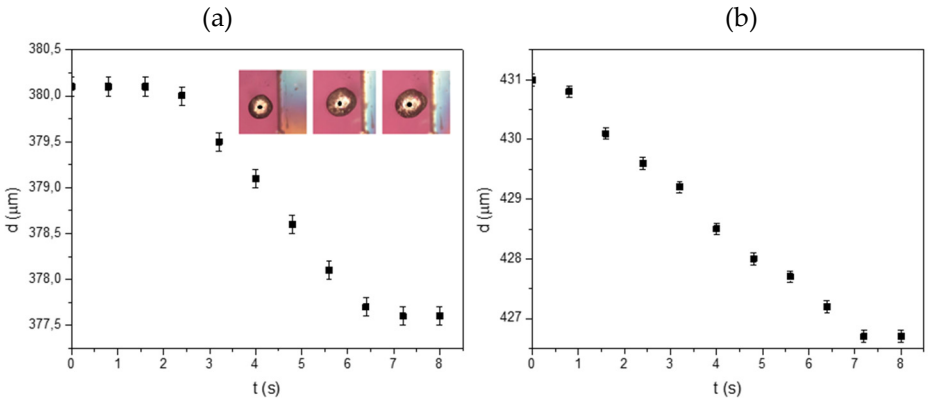

Figure 4. Distance of the droplet center (see text) from the edge of the LN slab, as a function of time in case of droplet lying on bare glass (**a**) and fluorolink-coated glass (**b**). The inset in Figure 4a shows the droplet in three different instants and helps in identifying the center (marked in black). The curve for bare glass suggests the presence of a pinning force that appears weaker in the case of fluorolink-coated glass substrate. Both curves show a linear trend, at least for a certain interval, indicating the presence of a dynamic friction dependent on the droplet velocity. Noteworthy, in case of fluorolink-coated substrate, the droplet center moves faster.

Results in Figure 4a suggest that the observed deformation in the direction of LN is due to the combination between an attractive force and a pinning force. Indeed, similar measurements performed on RM734 ferroelectric droplets lying on fluorolink-coated glass substrates, where the pinning force is expected to be quite low or even almost absent, show a much weaker droplet deformation toward LN and a displacement curve of a different initial shape. Specifically, keeping the cooling rate and the droplet size fixed, the motion starts well before 105 °C, namely right after the transition to the N_F phase, thus confirming a lower pinning force (Figure 4b).

The electromechanical instability is thus only one of the effects of the polarization coupling between the LC droplets and LN. This phenomenon occurs with different morphologies, as observed in [16], which might be due to various factors, including droplets' average diameter, different positions with respect to the LN crystal, variations in the instability temperature and different glass substrates. While we could not identify a clean connection between the observed morphologies and factors as the droplet diameter and instability temperature, we found that the glass substrate plays a specific role. Indeed, the instability observed on the fluorolink-coated glass results in thin jets that form a large number of secondary small droplets (see Figures 3 and 6 later on), in contrast to what happens on bare glass where the instability is characterized by the protrusion of large droplet areas combined with jets' ejection (Figure 2). We understand this difference as due to the different wettability of the two substrates. Indeed, fluorolink coating is known to substantially decrease the wettability of glass surfaces, thus favoring the formation of thin fluid jets and secondary droplets with respect to the ejection of fluid streams with large interfacial regions.

Despite the substrate used, the fluid jets ejected by RM734 droplets at instability poses a common feature. Indeed, they all exhibit the typical branched structure (Figures 2 and 3), which is due to their polarity and to charge accumulation on their tips [16]. By analyzing the evolution of this structure, we determined the Hausdorff (fractal) dimension d_f as a function of time, which is shown in Figure 5 for both droplets on bare and fluorolink-coated glass. In doing this, we selected a portion of a video where the branching of the ejected jets is easily visible, and determined d_f using the box counting method [28]. In both cases, d_f is lower than 2 and decreases to $d_f \cong 1.95$ as the time delay Δt from the initial frame increases. This indicates the fractal-like property of the formed structure [28,29].

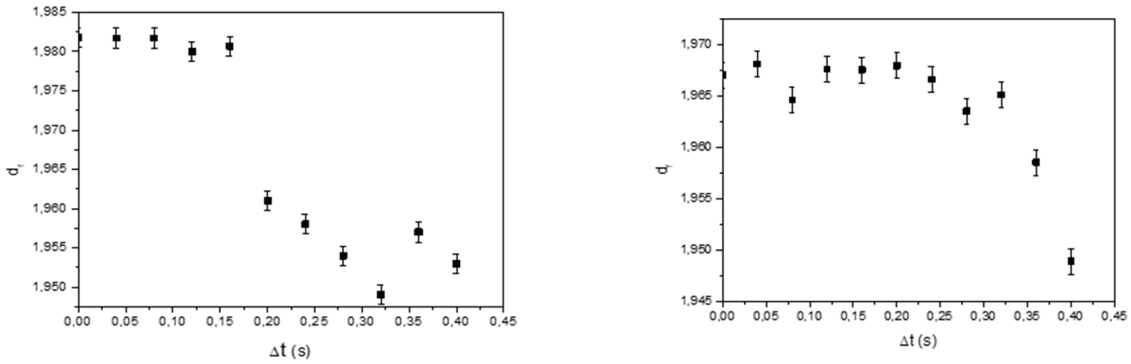

Figure 5. Hausdorff (fractal) dimension as a function of the time delay with respect to an initial video frame where the branched structure is beginning to form. The fractal dimension decreases as time passes, i.e., as the temperature decreases and the RM734 polarity increases. The dimension is always lower than 2 and decreases to $d_f \cong 1.95$, which demonstrates the fractal nature of jets' ramification.

As for the droplet position with respect to the LN crystal, we measured a maximum distance d_{MAX} between the droplet center and the LN edge beyond which the ferroelectric droplets are no longer affected by the polarization of the ferroelectric crystal. We found d_{MAX} = 500 µm for both kinds of glass substrates. We interpret this distance as the range of action of the fringing field generated by the pyroelectric charging of LN in our experimental conditions.

4. Discussion

Our results demonstrate that the coupling between the polarization of a ferroelectric droplet and the one of a ferroelectric solid, recently observed for ferroelectric sessile droplets on ferroelectric substrates [16,17], is possible even in conditions of no direct contact between the two materials. Such a coupling is mediated by the fringing field generated by the LN pyroelectric charging, in analogy to the case of ferroelectric droplets lying directly on LN substrates. The dependence of the effect on the initial distance between the droplet edge

and the LN border, observed here, is a clear demonstration of the role played by E_f. Indeed, E_f decreases with increasing the distance to the LN crystal so that if the initial distance between droplet edge and LN increases, the ferroelectric droplets experience a lower fringing field. This reasonably leads to a weaker overall effect, resulting in a less violent ejection of fluid jets and greater stability of the droplets' shape, which in fact undergoes deformation and electromechanical instability for lower values of T, corresponding to higher values of the polarization **P**.

The fringing field generated by the pyroelectric charging of the LN crystal affects the RM734 droplet in different ways. On the one hand, it induces the electromechanical instability leading to fluid jets' ejection, as reported in Figures 2, 3 and 6 and described in [16]. This means that the fringing field polarizes the ferroelectric droplet that thus rearranges its polarization **P** so as to cancel the internal field. In this process, opposite directions of **P** might nucleate and converge in specific locations of the droplets, forming topological defects that produce charge accumulation and act as triggers for jets' ejection [16]. On the other hand, it gives rise to an attractive force that we interpret as a dielectrophoretic force acting on the liquid crystal droplets, by pulling them toward the location corresponding to the maximum value of the fringing field amplitude [17]. It is known that the dielectrophoretic force F_{DEP} is due to the interaction between a non-uniform electric field and a polarizable dielectric material. In the simple case of spherical shape particles, F_{DEP} depends on the gradient of the electric field, squared as [30]:

$$F_{DEP} = 2\pi R^3 \varepsilon_m Re\left[\frac{\varepsilon_p - \varepsilon_m}{\varepsilon_p + 2\varepsilon_m}\right]\nabla E^2$$

where R is the radius of the spherical particle of complex dielectric permittivity ε_p, dispersed in a medium of complex dielectric permittivity ε_m. As discussed in [17], this expression can be used for ferroelectric sessile droplets with proper corrections to the Clausius–Mossotti ratio in square brackets, which can be approximated to unity, thus leading to a force dependent only on the droplet's radius and on the gradient of the field squared. Such a kind of force gives account for the observed droplet attraction toward the LN crystal.

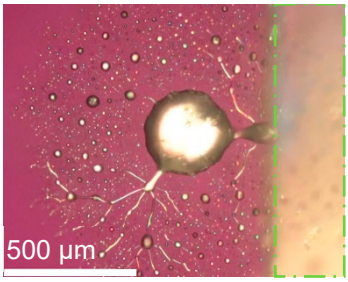

Figure 6. RM734 ferroelectric droplet on fluorolink-coated glass. The green dashed line marks the edge of an LN crystal positioned on the right-hand side of the droplet, initially at 200 µm from the droplet rim. The electromechanical instability results in the ejection of thin jets that disrupt by forming a huge number of small secondary droplets. A larger jet is instead directed toward the LN ferroelectric crystal and reaches its edge. Initial droplet diameter D = 308 µm; T = 100 °C.

The observed droplet deformation might be due to the combination between dielectrophoretic attraction and pinning, which also explains why it is lower in the case of fluorolink-coated substrates, where the pinning force is much weaker than on bare glass. However, this same deformation shows a sort of oscillatory behavior (see Video S1), which resembles the onset of an electromechanical instability. Indeed, as observed in Figure 2, jet ejection is generally preceded by droplet deformation that disappears as the jets are retracted by the original droplet. We thus interpret the observed droplet deformation as due to a combination of droplet motion driven by F_{DEP} but opposed by pinning, and shape instability driven by droplet polarization induced by the fringing field.

Noteworthy, due to the large droplet size, the fringing field is not uniform along the droplet diameter, that is, different regions of the droplet experience a different value of E_f. This reasonably affects both the field-induced instability and the dielectrophoretic interaction and contributes to the observed droplet deformation. Moreover, due to the dielectrophoretic attraction, internal fluid motion carrying material toward the droplet side closer to the LN edge might occur. This motion is expected to change the map of topological defects, displacing the regions of charge accumulation, thus making droplet instability and jet ejection much less controllable than in the experiments described in [16], where droplets are in direct contact with the whole charged area, and [17], where droplets are much smaller. In addition, the fluid jets themselves are most probably affected by F_{DEP} [18], which can result in a larger radius and a higher velocity of jets ejected close to LN, with respect to jets ejected from the other regions of the droplet rim, as shown in Figure 6 (extracted from Video S2 and available in the Supplementary Materials).

The described double action of the fringing field produced by the LN crystal indicates a double effect of the coupling between the polarizations of the fluid and solid materials. The two polarizations interact without the need of a direct contact, and this interaction has two results. Since large droplets have higher inertia with respect to small ones and since, according to [16], the temperature at which the electromechanical instability is observed decreases by decreasing the droplet diameter, it should be possible to select one of the two effects acting on the droplets' size. Specifically, the dielectrophoretic attraction should prevail in the case of small droplets, thus making droplet motion the dominant effect—in analogy to that observed in [17] for small ferroelectric droplets affected by the dielectrophoretic force generated because of the localized light-induced LN charging. On the contrary, in the case of large droplets, the electromechanical instability leading to jet ejection is expected to dominate over the droplet motion.

5. Conclusions

We demonstrated the existence of a coupling between the polarization of a ferroelectric fluid and the polarization of a ferroelectric solid, in conditions of no direct contact between the two materials. The coupling gives rise to two distinct effects: droplet polarization and consequent instability with the ejection of fluid jets, and dielectrophoretic-driven droplet motion toward the LN crystal. This latter is opposed by pinning, which can be decreased by using proper surface coatings and by decreasing the size of the contact line (i.e., the droplet perimeter), as well as by droplet inertia, which decreases as the droplet volume decreases. Therefore, the two effects can possibly be selected acting on the droplet size.

As the interaction between the two polarizations is mediated by the fringing field E_f that is generated by the pyroelectric effect in proximity of the ferroelectric crystal surface [16], our measurements set a value for the range of action of E_f in our experimental conditions.

The recent discovery of the ferroelectric nematic liquid crystals—the first ferroelectric fluids with a workable viscosity—is opening the gate to a whole new world of phenomena, all based on the peculiar combination of fluidity and polar coupling to electric fields, which are rapidly becoming the focus of the liquid crystal and soft material scientific communities. The results reported here are a step forward in the characterization and understanding of the coupling between the polarization of a ferroelectric fluid and the polarization of a ferroelectric solid, an effect completely unknown and unconceivable until just a few years ago.

Supplementary Materials: The following supporting materials can be downloaded at: https://www.mdpi.com/article/10.3390/cryst13050750/s1. Video S1 and Video S2.

Author Contributions: L.L. and R.B. conceived the experiment; S.B. made the measurements and analyzed data; L.L., R.B. and S.M. interpreted the results; L.L. wrote the manuscript; R.B. and L.L. prepared the figures. All the authors contributed to the final version. All authors have read and agreed to the published version of the manuscript.

Funding: Authors received no funding.

Institutional Review Board Statement: Not applicable.

Informed Consent Statement: Not applicable.

Data Availability Statement: All data are available upon request to the corresponding author.

Conflicts of Interest: Authors declare no conflict of interest.

References

1. Chen, X.; Korblova, E.; Dong, D.; Wei, X.; Shao, R.; Radzihovsky, L.; Glaser, M.A.; Maclennan, J.E.; Bedrov, D.; Walba, D.M.; et al. First-principles experimental demonstration of ferroelectricity in a thermotropic nematic liquid crystal: Polar domains and striking electro-optics. *Proc. Natl. Acad. Sci. USA* **2020**, *117*, 14021–14031. [CrossRef] [PubMed]
2. Born, M. Über anisotrope Flüssigkeiten. Versuch einer Theorie der flüssigen Kristalle und des elektrischen Kerr-Effekts in Flüssigkeiten. *Sitzungsber. Preuss. Akad Wiss.* **1916**, *30*, 614–650.
3. Lavrentovich, O.D. Ferroelectric nematic liquid crystal, a century in waiting. *Proc. Natl. Acad. Sci. USA* **2020**, *117*, 14629. [CrossRef] [PubMed]
4. Chen, X.; Korblova, E.; Glaser, M.A.; Maclennan, J.E.; Walba, D.M.; Clark, N.A. Polar in-plane surface orientation of a ferroelectric nematic liquid crystal: Polar monodomains and twisted state electro-optics. *Proc. Natl. Acad. Sci. USA* **2021**, *118*, e2104092118. [CrossRef]
5. Rudquist, P. Revealing the polar nature of a ferroelectric nematic by means of circular alignment. *Sci. Rep.* **2021**, *11*, 24411. [CrossRef]
6. Caimi, F.; Nava, G.; Barboza, R.; Clark, N.A.; Korblova, E.; Walba, D.M.; Bellini, T.; Lucchetti, L. Surface alignment of ferroelectric nematic liquid crystals. *Soft Matter* **2021**, *17*, 8130. [CrossRef]
7. Basnet, B.; Rajabi, M.; Wang, H.; Kumari, P.; Thapa, K.; Paul, S.; Lavrentovich, M.O. Soliton walls paired by polar surface interactions in a ferroelectric nematic liquid crystal. *O. D. Lavrentovich Nat. Commun.* **2022**, *13*, 3932. [CrossRef]
8. Mathè, M.T.; Buka, A.; Jakly, A.; Solomon, P. Ferroelectric nematic liquid crystal thermomotor. *Phys. Rev. E* **2022**, *105*, L052701. [CrossRef]
9. Cmok, L.; Coda, V.; Sebastián, N.; Mertelj, A.; Zgonik, M.; Aya, S.; Huang, M.; Montemezzani, G.; Drevenšek-Olenik, I. Running streams of a ferroelectric nematic liquid crystal on a lithium niobate surface. *Liq. Cryst.* **2023**. [CrossRef]
10. Sterle, A.; Cmok, L.; Sebastián, N.; Mertelj, A.; Kong, Y.; Zhang, X.; Drevenšek-Olenik, I. Light-induced dynamics of liquid-crystalline droplets on the surface of iron-doped lithium niobate crystals. *Opt. Mat. Exp.* **2023**, *13*, 282. [CrossRef]
11. Caimi, F.; Nava, G.; Fuschetto, S.; Lucchetti, L.; Paiè, P.; Osellame, R.; Chen, X.; Clark, N.A.; Glaser, M.; Bellini, T. Superscreening and polarization control in confined ferroelectric nematic liquids. *arXiv* **2018**, arXiv:2210.00886.
12. Kumari, P.; Basnet, B.; Wang, H.; Lavrentovich, O.D. Hidden chemical order in disordered Ba7Nb4MoO20 revealed by resonant X-ray diffraction and solid-state NMR. *Nat. Comm.* **2023**, *14*, 748. [CrossRef] [PubMed]
13. Sebastián, N.; Lovšin, M.; Berteloot, B.; Osterman, N.; Petelin, A.; Mandle, R.J.; Aya, S.; Huang, M.; Drevenšek-Olenik, I.; Neyts, K.; et al. Polarization patterning in ferroelectric nematic liquids. *arXiv* **2023**, arXiv:2301.07933v1.
14. Yu, J.-S.; Lee, J.H.; Lee, J.-Y.; Kim, J.-H. Alignment properties of a ferroelectric nematic liquid crystal on the rubbed substrates. *Soft Matter* **2023**, *19*, 2446–2453. [CrossRef]
15. Perera, K.; Saha, R.; Nepal, P.; Dharmarathna, R.; Hossain, M.S.; Mostafa, M.; Adaka, A.; Waroquet, R.; Twiegd, R.J.; Jákli, A. Ferroelectric nematic droplets in their isotropic melt. *Soft Matter* **2023**, *19*, 347–354. [CrossRef]
16. Barboza, R.; Marni, S.; Ciciulla, F.; Mir, F.A.; Nava, G.; Caimi, F.; Zaltron, A.; Clark, N.; Bellini, T.; Lucchetti, L. Explosive Electrostatic Instability of Ferroelectric Liquid Droplets on Ferroelectric Solid Surfaces. *Proc. Natl. Acad. Sci. USA* **2022**, *119*, e2207858119. [CrossRef]
17. Marni, S.; Nava, G.; Barboza, R.; Bellini, T.; Lucchetti, L. Walking Ferroelectric Liquid Droplets with Light. *Adv. Mater.* **2023**. [CrossRef]
18. Marni, S.; Barboza, R.; Lucchetti, L. Optical Control Of Mass Ejection From Ferroelectric Liquid Droplets: A Possible Tool For The Actuation Of Complex Fluids. *arXiv* **2023**, arXiv:2303.14798.
19. Habibpourmoghadam, A.; Lucchetti, L.; Evans, D.; Reshetnyak, V.; Omairat, F.; Schafforz, S.L.; Lorenz, A. Laser-induced erasable patterns in a N* liquid crystal on an iron doped lithium niobate surface. *Opt. Express* **2017**, *25*, 26148. [CrossRef]
20. Lucchetti, L.; Kushnir, K.; Zaltron, A.; Simoni, F.J. Self-activating liquid crystal devices for smart laser protection. *Eur. Opt. Soc.* **2016**, *116*, 16007. [CrossRef]
21. Ciciulla, F.; Zaltron, A.; Zamboni, R.; Sada, C.; Simoni, F.; Reshetnyak, V.; Lucchetti, L. Optofluidic platform based on liquid crystals in X-Cut lithium niobate: Thresholdless all-optical response. *Crystals* **2021**, *11*, 908. [CrossRef]
22. Schafforz, S.L.; Nordendorf, G.; Nava, G.; Lucchetti, L.; Lorenz, A. Formation of relocatable umbilical defects in a liquid crystal with positive dielectric anisotropy induced via photovoltaic fields. *J. Mol. Liq.* **2020**, *307*, 112963. [CrossRef]
23. Sanna, S.; Schmidt, W. G LiNbO3 surfaces from a microscopic perspective. *J. Phys. Condens. Matter* **2017**, *29*, 413001–4130048. [CrossRef] [PubMed]

24. Kostritskii, S.M.; Sevostyanov, O.G.; Bourson, M.A.P. Non-linear light scattering in photorefractive LiNbO3 crystals studied by Z-scan technique. *J. Appl. Phys.* **2008**, *104*, 114104–114111. [CrossRef]
25. Byer, R.L.; Roundy, C.B. Pyroelectric coefficient direct measurement technique and application to a nsec response time detector. *Ferroelectrics* **2011**, *2011*, 333–338.
26. Bonfadini, S.; Ciciulla, F.; Criante, L.; Zaltron, A.; Simoni, F.; Reshetnyak, V.; Lucchetti, L. Optofluidic platform using liquid crystals in lithium niobate microchannel. *Sci. Rep.* **2019**, *9*, 1062–1067.
27. Gebre, T.; Batra, A.K.; Guggilla, P.; Aggarwal, M.D.; Lal, R.B. Pyroelectric properties of pure and doped lithium niobate crystals for infrared sensors. *Ferroelectr. Lett. Sect.* **2010**, *31*, 131–139. [CrossRef]
28. Dierking, I. Liquid crystals, fractals and art. *Liq. Cryst. Today* **2012**, *21*, 54–65. [CrossRef]
29. Marcell Tibor Máthé, Bendegúz Farkas, László Péter, Ágnes Buka, Antal Jákli1, Péter Salamon, Electric feld-induced interfacial instability in a ferroelectric nematic liquid crystal, Sci. *Rep.* **2023**, *13*, 6981.
30. Sarno, B.; Heineck, D.; Heller, M.J.; Ibsen, S.D. Dielectrophoresis: Developments and applications from 2010 to 2020. *Electrophoresis* **2021**, *42*, 539. [CrossRef]